Constraints on lepton universality violation from rare *B* decays

Marco Ciuchini,[1,*] Marco Fedele,[2,†] Enrico Franco,[3,‡] Ayan Paul,[4,§] Luca Silvestrini,[3,‖] and Mauro Valli[3,5,¶]

[1]*INFN Sezione di Roma Tre, Via della Vasca Navale 84, I-00146 Rome, Italy*
[2]*Institut für Theoretische Teilchenphysik, Karlsruhe Institute of Technology, D-76131 Karlsruhe, Germany*
[3]*INFN Sezione di Roma, Piazzale Aldo Moro 2, I-00185 Rome, Italy*
[4]*Electrical and Computer Engineering, Northeastern University, Boston, Massachusetts 02115, USA*
[5]*C.N. Yang Institute for Theoretical Physics, Stony Brook University, Stony Brook, New York 11794, USA*

(Received 17 January 2023; accepted 10 March 2023; published 23 March 2023)

The LHCb Collaboration has recently released a new study of $B^+ \to K^+\ell^+\ell^-$ and $B \to K^{*0}\ell^+\ell^-$ ($\ell = e, \mu$) decays, testing lepton universality with unprecedented accuracy using the whole Run 1 and 2 dataset. In addition, the CMS Collaboration has reported an improved analysis of the branching ratios $B_{(d,s)} \to \mu^+\mu^-$. While these measurements offer, *per se*, a powerful probe of new physics, global analyses of $b \to s\ell^+\ell^-$ transitions also rely on the assumptions about nonperturbative contributions to the decay matrix elements. In this work, we perform a global Bayesian analysis of new physics in (semi)leptonic rare *B* decays, paying attention to the role of charming penguins which are difficult to evaluate from first principles. We find data to be consistent with the Standard Model once rescattering from intermediate hadronic states is included. Consequently, we derive stringent bounds on lepton universality violation in $|\Delta B| = |\Delta S| = 1$ (semi)leptonic processes.

DOI: 10.1103/PhysRevD.107.055036

Since the first collisions in 2010, the Large Hadron Collider (LHC) allowed for a tremendous step forward in the electroweak (EW) sector of the Standard Model (SM) of particle physics—culminated with the discovery of the Higgs boson [1,2]—while it has also excited the community with a few interesting hints of physics beyond the SM (BSM). In particular, the LHCb Collaboration provided the first statistically relevant hint for lepton universality violation (LUV) in flavor-changing neutral-current (FCNC) processes [3], measuring the ratio $R_K \equiv \mathrm{Br}(B^+ \to K^+\mu^+\mu^-)/\mathrm{Br}(B^+ \to K^+e^+e^-)$ in the dilepton invariant-mass range $q^2 \in [1, 6]\ \mathrm{GeV}^2$. These hints have been confirmed by subsequent measurements, always by the LHCb Collaboration, namely R_K [4], R_{K^*} [5,6], R_{K_S}, and $R_{K^{*+}}$ [7].

Interestingly enough, these hints of LUV appeared in transitions where deviations from the SM were already claimed, see e.g., [8–11], on the basis of the measurements of angular distributions in $b \to s\mu^+\mu^-$ decays [12–23]. Claiming discrepancies from SM predictions in branching ratios (BRs) and angular distributions requires, however, full theoretical control on hadronic uncertainties in the matrix element calculation [24–26], and in particular on the so-called charming penguins [27], which might affect the vector coupling to the leptons even in regions of the dilepton invariant mass well below the charmonium threshold [28,29] and bring the SM in agreement with experiment [30]. Combining angular distributions with LUV data strengthened the case for new physics (NP), since a single NP contribution could reproduce the whole set of data [31–39]. On the other hand, charming penguins might affect the picture of NP behind LUV, since LUV ratios depend on the interplay of NP and hadronic contributions [38,40–42]. While considerable progress has been made in estimating (at least part of) the charming-penguin amplitudes using light cone sum rules [43,44] and analyticity supplemented with perturbative QCD in the Euclidean q^2 region [45–48], calculating these hadronic contributions remains an open problem, as we discuss below.

Before presenting our results, we notice that at the end of 2022 the experimental picture drawn so far has suddenly changed. Firstly, the CMS Collaboration provided a new analysis of $\mathrm{BR}(B_{(d,s)} \to \mu^+\mu^-)$ with the full Run 2 dataset [49], bringing the HFLAV average

$$\mathrm{BR}(B_s \to \mu^+\mu^-) = (3.45 \pm 0.29) \times 10^{-9} \qquad (1)$$

*marco.ciuchini@roma3.infn.it
†marco.fedele@kit.edu
‡enrico.franco@roma1.infn.it
§a.paul@northeastern.edu
‖luca.silvestrini@roma1.infn.it
¶mauro.valli@roma1.infn.it

into excellent agreement with the SM prediction $\mathrm{BR}(B_s \to \mu^+\mu^-) = (3.47 \pm 0.14) \times 10^{-9}$ [50,51]. Being short-distance dominated, this FCNC process strongly constrains NP contributions involving, in particular, axial leptonic couplings [52,53]. Furthermore, an updated LHCb analysis of R_K and R_{K^*} based on the full Run 1 and 2 dataset has been presented [54,55],

$$\begin{aligned} R_{K_{[0.1,1.1]}} &= 0.994^{+0.090}_{-0.082}(\mathrm{stat})\,^{+0.029}_{-0.027}(\mathrm{syst}), \\ R_{K^*_{[0.1,1.1]}} &= 0.927^{+0.093}_{-0.087}(\mathrm{stat})\,^{+0.036}_{-0.035}(\mathrm{syst}), \\ R_{K_{[1.1,6]}} &= 0.949^{+0.042}_{-0.041}(\mathrm{stat})\,^{+0.022}_{-0.022}(\mathrm{syst}), \\ R_{K^*_{[1.1,6]}} &= 1.027^{+0.072}_{-0.068}(\mathrm{stat})\,^{+0.027}_{-0.026}(\mathrm{syst}), \end{aligned} \tag{2}$$

with correlations reported in Fig. 26 of Ref. [55]. These new measurements dramatically change the scenario of possible LUV effects in FCNC B decays [56], questioning what in the last years served as fertile ground for model building, see for instance [57–81].

In this paper we provide a reassessment of NP effects in $b \to s\mu^+\mu^-$ transitions in view of the experimental novelties discussed above. Adopting the model-independent language of the Standard Model effective theory (SMEFT) [82,83], we present an updated analysis of $|\Delta B| = |\Delta S| = 1$ (semi)leptonic processes and show that current data no longer provide strong hints for NP. Indeed, updating the list of observables considered in our previous global analysis [38] with the results in Eqs. (1) and (2), the only remaining measurements deviating from SM expectations and not affected by hadronic uncertainties are the LUV ratios R_{K_S} and $R_{K^{*+}}$ [7], for which a reanalysis by the LHCb Collaboration is mandatory in view of what discussed in [54,55].

The anatomy of the $B \to K^{(*)}\ell^+\ell^-$ decay can be characterized in terms of helicity amplitudes [24,84], that in the SM at a scale close to the bottom quark mass m_b can be written as

$$\begin{aligned} H_V^\lambda &\propto \left\{ C_9^{\mathrm{SM}} \tilde{V}_{L\lambda} + \frac{m_B^2}{q^2}\left[\frac{2m_b}{m_B} C_7^{\mathrm{SM}} \tilde{T}_{L\lambda} - 16\pi^2 h_\lambda\right]\right\}, \\ H_A^\lambda &\propto C_{10}^{\mathrm{SM}} \tilde{V}_{L\lambda}, \qquad H_P \propto \frac{m_\ell m_b}{q^2} C_{10}^{\mathrm{SM}} \left(\tilde{S}_L - \frac{m_s}{m_b}\tilde{S}_R\right), \end{aligned}$$

with $\lambda = 0, \pm$ and $C_{7,9,10}^{\mathrm{SM}}$ the SM Wilson coefficients of the semileptonic operators of the $|\Delta B| = |\Delta S| = 1$ weak effective Hamiltonian [85–87], normalized as in Ref. [41]. The naively factorizable contributions to the above amplitudes can be expressed in terms of seven q^2-dependent form factors, $\tilde{V}_{0,\pm}$, $\tilde{T}_{0,\pm}$ and $\tilde{S}$ [88,89]. At the loop level, nonlocal effects parametrically not suppressed (neither by small Wilson coefficients nor by small CKM factors) arise from the insertion of the following four-quark operator:

$$Q_2^c = (\bar{s}_L \gamma_\mu c_L)(\bar{c}_L \gamma^\mu b_L), \tag{3}$$

that yields nonfactorizable power corrections in H_V^λ via the hadronic correlator $h_\lambda(q^2)$ [26,30,90], receiving the main contribution from the time-ordered product,

$$\frac{\epsilon_\mu^*(\lambda)}{m_B^2} \int d^4x e^{iqx} \langle \bar{K}^* | \mathcal{T}\{ j_{\mathrm{em}}^\mu(x) Q_2^c(0)\} | \bar{B}\rangle, \tag{4}$$

with $j_{\mathrm{em}}^\mu(x)$ the electromagnetic (quark) current.

This correlator receives two kinds of contributions. The first corresponds to diagrams of the form of diagram (a) in Fig. 1, where the initial B meson decays to the $K^{(*)}$ plus a $c\bar{c}$ state that subsequently goes into a virtual photon. This contribution has been studied in detail in the context of light cone sum rules in the regime $q^2 \ll 4m_c^2$ in [43]; in the same reference, dispersion relations were used to extend the result to larger values of the dilepton invariant mass. While the operator product expansion performed in Ref. [43] was criticized in Ref. [29], and multiple soft-gluon emission may represent an obstacle for the correct evaluation of this class of hadronic contributions [30,40,91,92], Refs. [45,46] have exploited analyticity in a more refined way than [43]. In those works the negative q^2 region—where perturbative

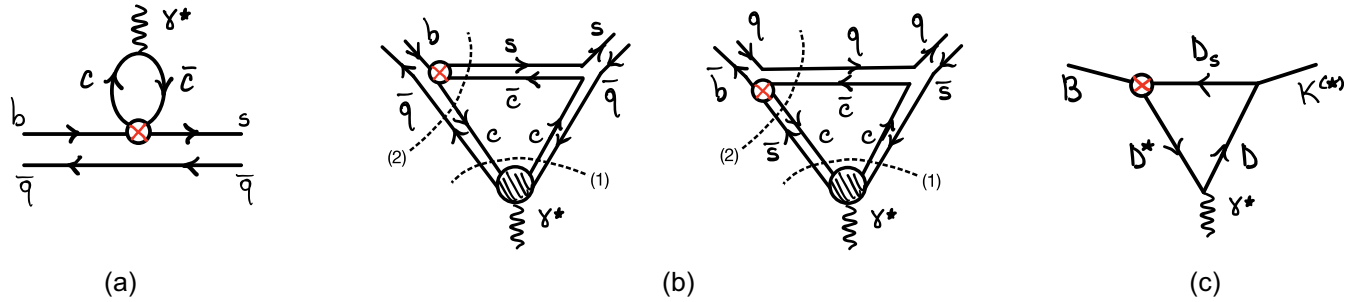

FIG. 1. Example of charming-penguin diagrams contributing to the $B \to K^{(*)}\ell^+\ell^-$ amplitude. Diagram (a) represents the class of charming-penguin amplitudes related to $c - \bar{c}$ state that subsequently goes into a virtual photon, see Refs. [43,45–48]. Diagrams (b) and (c) represent the kind of contributions from rescattering of intermediate hadronic states, at the quark and meson level respectively. The phenomenological relevance of rescattering for the SM prediction of the $B \to K^{(*)}\ell^+\ell^-$ decays has been recently considered in Ref. [38].

QCD is supposed to be valid—has been used to further constrain the amplitude. Building on these works, together with unitarity bounds [47], Ref. [48] found a very small effect in the large-recoil region.

The second kind of contribution to the correlator in Eq. (4) originates from the triangle diagrams depicted in Fig. 1(b), in which the photon can be attached both to the quark and antiquark lines and we have not drawn explicitly the gluons exchanged between quark-antiquark pairs. An example of an explicit hadronic contribution of this kind is depicted in Fig. 1(c).[1] The $D_s D^*$ pair is produced by the weak decay of the initial B meson with low momentum, so that no color transparency argument holds and rescattering can easily take place. Furthermore, the recent observation of tetraquark states in $e^+e^- \to K(D_s D^* + D_s^* D)$ by the BESIII Collaboration [94] confirms the presence of nontrivial nonperturbative dynamics of the intermediate state.

One could think of applying dispersive methods also to this kind of contributions, but the analytic structure of triangle diagrams is quite involved, depending on the values of external momenta and internal masses. A dispersion relation in q^2 of the kind used in Refs. [43,45–48], based on the cut denoted by (1) in Fig. 1(b), could be written if the B invariant mass were below the threshold for the production of charmed intermediate states. However, when the B invariant mass raises above the threshold for cut (2), an additional singularity moves into the q^2 integration domain, requiring a nontrivial deformation of the path (see for example the detailed discussion in Ref. [95]). Another possibility would be to get an order-of-magnitude estimate of contributions as the one in Fig. 1(c) using an approach similar to Ref. [93].

To be conservative, and in the absence of a first-principle calculation of the diagrams in Fig. 1, we adopt a data-driven approach based on the following parametrization of the hadronic contributions, inspired by the expansion of the correlator of Eq. (4) as originally done in Ref. [24], and worked out in detail in Ref. [92],

$$
\begin{aligned}
H_V^- &\propto \frac{m_B^2}{q^2}\left[\frac{2m_b}{m_B}(C_7^{\rm SM}+h_-^{(0)})\tilde{T}_{L-} - 16\pi^2 h_-^{(2)} q^4\right] \\
&\quad + (C_9^{\rm SM}+h_-^{(1)})\tilde{V}_{L-}, \\
H_V^+ &\propto \frac{m_B^2}{q^2}\left[\frac{2m_b}{m_B}(C_7^{\rm SM}+h_-^{(0)})\tilde{T}_{L+} - 16\pi^2 (h_+^{(0)} \right. \\
&\quad \left. + h_+^{(1)} q^2 + h_+^{(2)} q^4)\right] + (C_9^{\rm SM}+h_-^{(1)})\tilde{V}_{L+}, \\
H_V^0 &\propto \frac{m_B^2}{q^2}\left[\frac{2m_b}{m_B}(C_7^{\rm SM}+h_-^{(0)})\tilde{T}_{L0} - 16\pi^2 \sqrt{q^2}(h_0^{(0)} + h_0^{(1)} q^2)\right] \\
&\quad + (C_9^{\rm SM}+h_-^{(1)})\tilde{V}_{L0}. \qquad (5)
\end{aligned}
$$

[1]See Ref. [93] for a very recent estimate of similar diagrams with up quarks, rather than charm quarks, in the internal loop.

This parametrization—while merely rooted on a phenomenological basis—has the advantage of making transparent the interplay between hadronic and possible NP contributions. Indeed, the coefficients $h_-^{(0)}$ and $h_-^{(1)}$ have the same effect of a lepton universal shift due to NP in the real part of the Wilson coefficients C_7 and C_9, respectively. Consequently, the theoretical assumptions on the size of these hadronic parameters crucially affect the extraction of NP contributions to $C_{7,9}$ from global fits. Within the SM, the new measurements in Eqs. (1) and (2) do not affect the knowledge of the h_λ coefficients; the most up-to-date data-driven extraction of the hadronic parameters introduced in Eq. (5) can be found in Table 1 of Ref. [38]. See the Appendix for further details regarding the hadronic parametrization employed in the data-driven approach.

Moving to the analysis of NP, current constraints from direct searches at the LHC reasonably suggest in this context that BSM physics would arise at energies much larger than the electroweak scale. Then, a suitable framework to describe such contributions is given by the SMEFT, in particular by adding to the SM the following dimension-six operators[2]:

$$
\begin{aligned}
O_{2223}^{LQ^{(1)}} &= (\bar{L}_2\gamma_\mu L_2)(\bar{Q}_2\gamma^\mu Q_3), \\
O_{2223}^{LQ^{(3)}} &= (\bar{L}_2\gamma_\mu \tau^A L_2)(\bar{Q}_2\gamma^\mu \tau^A Q_3), \\
O_{2322}^{Qe} &= (\bar{Q}_2\gamma_\mu Q_3)(\bar{e}_2\gamma^\mu e_2), \\
O_{2223}^{Ld} &= (\bar{L}_2\gamma_\mu L_2)(\bar{d}_2\gamma^\mu d_3), \\
O_{2223}^{ed} &= (\bar{e}_2\gamma_\mu e_2)(\bar{d}_2\gamma^\mu d_3), \qquad (6)
\end{aligned}
$$

where in the above $\tau^{A=1,2,3}$ are Pauli matrices, a sum over A is understood, L_i and Q_i are $SU(2)_L$ doublets, e_i and d_i singlets, and flavor indices are defined in the basis where the down-quark Yukawa matrix is diagonal. For concreteness, we normalize SMEFT Wilson coefficients to a NP scale $\Lambda_{\rm NP} = 30$ TeV and we only consider NP contributions to muons.[3] The matching between the weak effective Hamiltonian and the SMEFT operators implies the following contributions to the SM operators and to the chirality-flipped ones denoted by primes [98]:

$$
\begin{aligned}
C_9^{\rm NP} &= \mathcal{N}_\Lambda(C_{2223}^{LQ^{(1)}} + C_{2223}^{LQ^{(3)}} + C_{2322}^{Qe}), \\
C_{10}^{\rm NP} &= \mathcal{N}_\Lambda(C_{2322}^{Qe} - C_{2223}^{LQ^{(1)}} - C_{2223}^{LQ^{(3)}}), \\
C_9^{\prime,\rm NP} &= \mathcal{N}_\Lambda(C_{2223}^{ed} + C_{2223}^{Ld}), \\
C_{10}^{\prime,\rm NP} &= \mathcal{N}_\Lambda(C_{2223}^{ed} - C_{2223}^{Ld}), \qquad (7)
\end{aligned}
$$

[2]Note that these operators may be generated via renormalization group effects, see, e.g., Refs. [96,97].

[3]This choice is mainly motivated by the fact that $B_s \to \mu^+\mu^-$ is one of the key observables of the present study.

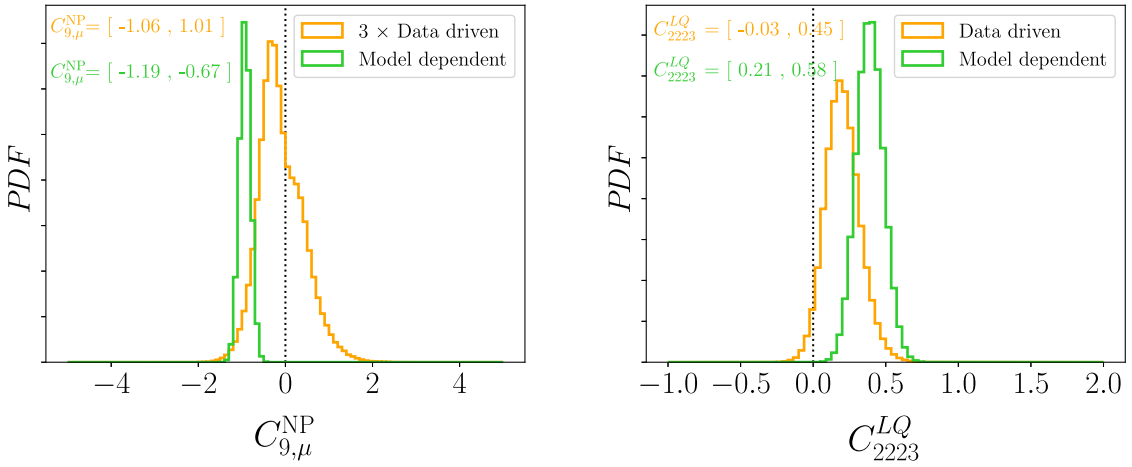

FIG. 2. Left panel: Posterior PDF for the NP coefficient $C^{\rm NP}_{9,\mu}$. Right panel: Posterior PDF for the SMEFT Wilson coefficient C^{LQ}_{2223}. For both panels, we show the PDF in green and orange on the basis of the hadronic approach adopted in the global analysis (see the text for more details).

with $\mathcal{N}_\Lambda = (\pi v^2)/(\alpha_e V_{ts} V^*_{tb} \Lambda^2_{\rm NP})$. As evident from the above equation, operators $O^{LQ^{(1,3)}}_{2223}$ always enter as a sum. Hence we denote their Wilson coefficient as C^{LQ}_{2223}.

We perform a Bayesian fit to the data in Refs. [13, 17–23,49,54,55,99–105] employing the HEPfit code [106,107]. For the form factors and input parameters, we follow the same approach used in our previous Refs. [30,38,40–42,91,92]. In particular, we use the same inputs as in Ref. [38], with the only exception of CKM parameters, which have been updated according to the results of Ref. [51]. We compute $B \to K^{(*)}\ell^+\ell^-$ and $B_s \to \phi\ell^+\ell^-$ decays using QCD factorization [108].

As already mentioned discussing Fig. 1, a global analysis of $b \to s\ell^+\ell^-$ transitions can be sensitive to hadronic contributions that are difficult to compute from first principles and that can yield important phenomenological effects. Therefore, in what we denote below as data-driven scenario, we assume a flat prior in a sufficiently large range for the $h^{(0,1,2)}_\pm$ and $h^{(0,1)}_0$ parameters, which are then determined from data simultaneously with the NP coefficients.[4] To clarify the phenomenological relevance of charming penguins, we compare the results of the data-driven approach against what we denote instead as model-dependent treatment of hadronic uncertainties, in which we assume that the contributions generated by the diagrams in Fig. 1(b) (or 1(c)) are negligible and that the correlator in Eq. (4) is well described by the approach of Refs. [43–48], yielding a subleading effect to the hadronic effects computable in QCD factorization. See the Appendix for further details regarding the parametrization of hadronic contributions employed in the model-dependent approach.

[4]As in Ref. [38], we assume exact SU(3) flavor for the h parameters and add additional ones for $B \to K$.

In both approaches to QCD long-distance effects, we obtain a sample of the posterior joint probability density function (PDF) of SM parameters, including form factors, and, in the data-driven scenario, h_λ parameters, together with NP Wilson coefficients. From each posterior PDF we compute the highest probability density intervals (HPDIs), which represent our best knowledge of the model parameters after the new measurements. We also perform model comparison using the information criterion [109], defined as

$$\mathrm{IC} \equiv -2\overline{\log \mathcal{L}} + 4\sigma^2_{\log \mathcal{L}}, \tag{8}$$

where the first and second terms are the mean and variance of the log-likelihood posterior distribution. The first term

TABLE I. HPDI for the Wilson coefficients of the low-energy weak Hamiltonian in all the considered NP scenarios along with the corresponding ΔIC. Results obtained in the data-driven scenario are given in roman, while model-dependent scenario results are highlighted in bold. See the text for the definition of the two scenarios.

	95% HPDI	ΔIC
$C^{\rm NP}_{9,\mu}$	[−1.06, 1.01]	−2.4
	[−1.19, −0.67]	**43**
$\{C^{\rm NP}_{9,\mu}, C^{\rm NP}_{10,\mu}\}$	{[−0.83, 1.06], [−0.07, 0.43]}	−3.4
	{[−1.22, −0.70],[−0.37,0.00]}	**41**
$\{C^{\rm NP}_{9,\mu}, C'^{\rm NP}_{9,\mu}\}$	{[−1.06, 1.40], [−2.20, 1.31],	−4.1
	{[−1.33, −0.79],[0.08,0.88],	**45**
$\{C^{\rm NP}_{9,\mu}, C'^{\rm NP}_{10,\mu}\}$	{[−1.07, 1.20], [−0.28, 0.20],	−5.1
	{[−1.34, −0.77],[−0.39,0.02],	**41**
$\{C^{\rm NP}_{9,\mu}, C^{\rm NP}_{10,\mu}, C'^{\rm NP}_{9,\mu}, C'^{\rm NP}_{10,\mu}\}$	{[−0.90, 1.49], [−0.15, 0.62], [−2.27, 1.18], [−0.33, 0.47]}	−8.1
	{[−1.38, −0.82],[−0.39,0.02], [−0.49,0.79],[−0.46,0.17]}	**57**

TABLE II. Same as Table I for SMEFT Wilson coefficients.

	95% HPDI	ΔIC
C_{2223}^{LQ}	[−0.03, 0.45]	−1.6
	[0.21, 0.58]	**3**
$\{C_{2223}^{LQ}, C_{2322}^{Qe}\}$	$\{[-0.59, 0.64], [-0.94, 0.54]\}$	−3.4
	$\{$**[0.34,0.73]**,**[0.55,1.04]**$\}$	**41**
$\{C_{2223}^{LQ}, C_{2223}^{ed}\}$	$\{[-0.03, 0.48], [-0.39, 0.32]\}$	−4.0
	$\{$**[0.24,0.63]**,**[−0.95,−0.09]**$\}$	**6**
$\{C_{2223}^{LQ}, C_{2223}^{Ld}\}$	$\{[-0.06, 0.65], [-0.24, 0.49]\}$	−5.1
	$\{$**[0.18,0.57]**,**[−0.14,0.23]**$\}$	**−2**
$\{C_{2223}^{LQ}, C_{2322}^{Qe}, C_{2223}^{Ld}, C_{2223}^{ed}\}$	$\{[-0.88, 0.78], [-1.26, 0.57], [-0.76, 1.58], [-0.98, 1.64]\}$	−8.1
	$\{$**[0.43,0.84]**,**[0.62,1.16]**, **[−0.50,0.10]**,**[−0.64,0.63]**$\}$	**57**

measures the quality of the fit, while the second one is related to the effective degrees of freedom involved, penalizing more complicated models. Models with smaller IC should then be preferred [110]. While the posterior distributions for SM parameters are unaffected by LUV measurements, the SM IC of course depends on the latter; indeed, the SM in the data-driven scenario provides an excellent description of current data, leading to slightly negative values of $\Delta\mathrm{IC} \equiv \mathrm{IC}_{\mathrm{SM}} - \mathrm{IC}_{\mathrm{NP}}$. Conversely, the agreement of the SM with angular observables remains poor in the model-dependent approach, implying for this case large values of ΔIC, signaling a statistically significant preference for NP.

We now discuss several NP configurations, in order of increasing complexity. We start by allowing a single novanishing NP Wilson coefficient, either $C_{9,\mu}^{\mathrm{NP}}$, defined in the low-energy weak Hamiltonian, or the Wilson coefficient C_{2223}^{LQ}, belonging to the SMEFT. The PDFs for the two NP Wilson coefficients are reported in Fig. 2, while the corresponding numerical results for the 95% HPDIs are reported in the first row of Tables I and II. As anticipated above, no significant preference for NP is seen in the data-driven scenario, while NP contributions are definitely needed in the model-dependent scenario, with a clear preference for $C_{9,\mu}^{\mathrm{NP}} \neq 0$.

Figure 3 displays the allowed regions in the $C_{9,\mu}^{\mathrm{NP}} - C_{10,\mu}^{\mathrm{NP}}$ and $C_{2223}^{LQ} - C_{2322}^{Qe}$ planes, while the corresponding HPDIs are reported in the second row of Tables I and II, respectively. Again, no evidence for NP is seen in the data-driven case, while clear evidence for a nonvanishing $C_{9,\mu}^{\mathrm{NP}}$ appears in the model-dependent approach. Deviations from zero of $C_{10,\mu}^{\mathrm{NP}}$ are strongly constrained by $\mathrm{BR}(B_s \to \mu^+\mu^-)$, corresponding to the strong correlation $C_{2223}^{LQ} \sim C_{2322}^{Qe}$ seen in the right panel of Fig. 3.

Next, we consider NP models in which right-handed $b \to s$ transitions arise. In the weak effective Hamiltonian, we allow for nonvanishing $C_{9,\mu}^{\mathrm{NP}}$ and $C_{9,\mu}^{\prime,\mathrm{NP}}$ or $C_{10,\mu}^{\prime,\mathrm{NP}}$. In particular, in Fig. 4 we present the results of the fit in the $C_{9,\mu}^{\mathrm{NP}} - C_{10,\mu}^{\prime,\mathrm{NP}}$ case, which we considered in Ref. [41] as the best fit one in view of the deviation from one of the ratio R_K/R_{K^*} [111]. With the current experimental situation, this is not the case anymore, and $C_{10,\mu}^{\prime,\mathrm{NP}}$ is again strongly constrained by $\mathrm{BR}(B_s \to \mu^+\mu^-)$. In the SMEFT, we consider nonvanishing C_{2223}^{LQ} and C_{2223}^{ed} or C_{2223}^{Ld}. The numerical results for the NP coefficients can be found in the third and fourth rows of Tables I and II.

Finally, we present in Fig. 5 the results of a combined fit in which all the four NP Wilson coefficients considered above are allowed to float simultaneously, namely C_{2223}^{LQ}, C_{2322}^{Qe}, C_{2223}^{Ld}, and C_{2223}^{ed}, or equivalently, in the language of the weak effective Hamiltonian, $C_{9,\mu}^{\mathrm{NP}}$, $C_{10,\mu}^{\mathrm{NP}}$ and the corresponding operators with right-handed quark currents $C_{9,\mu}^{\prime,\mathrm{NP}}$, $C_{10,\mu}^{\prime,\mathrm{NP}}$. Several interesting features emerge in this fit. First,

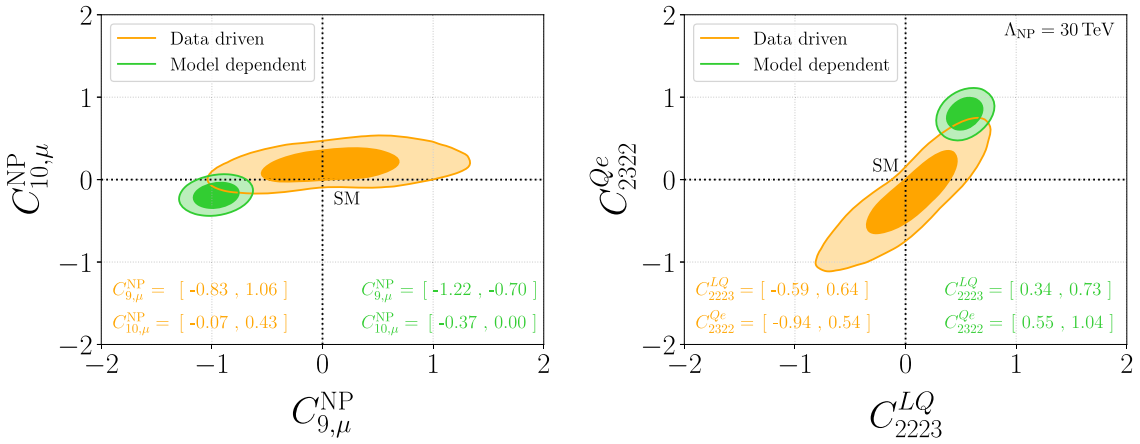

FIG. 3. Left panel: Joint posterior PDF for $C_{9,\mu}^{\mathrm{NP}}$ and $C_{10,\mu}^{\mathrm{NP}}$. Right panel: Joint posterior PDF for the SMEFT Wilson coefficients C_{2223}^{LQ} and C_{2322}^{Qe}. For both panels, we show 68% and 95% probability regions in green and orange on the basis of the hadronic approach adopted in the global analysis (see the text for more details).

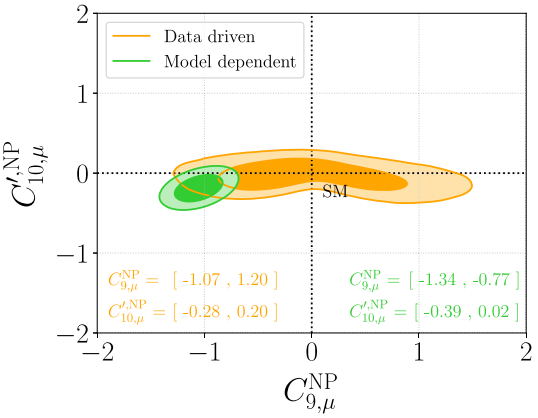

FIG. 4. Joint posterior PDF for $C^{\rm NP}_{9,\mu}$ and $C^{\prime,\rm NP}_{10,\mu}$. We show 68% and 95% probability regions in green and orange on the basis of the hadronic approach adopted in the global analysis (see the text for more details).

the updated experimental value of $\mathrm{BR}(B_s \to \mu^+\mu^-)$ forces $C^{\rm NP}_{10,\mu}$ and $C^{\prime,\rm NP}_{10,\mu}$ to be small, corresponding to the correlations visible in the two-dimensional projections on the C^{LQ}_{2223} vs C^{Qe}_{2322} and C^{Ld}_{2223} vs C^{ed}_{2223} planes and reported in Fig. 6. Second, the SM point is well inside the 68% probability regions in the data-driven approach, while in the model-dependent scenario there is evidence of a nonvanishing $C^{\rm NP}_{9,\mu}$, or equivalently of a nonvanishing $C^{LQ}_{2223} \sim C^{Qe}_{2322}$, stemming from BRs and angular distributions of $b \to s\mu^+\mu^-$ transitions. In the data-driven scenario the latter are reproduced thanks to the charming penguin contributions. Eventually, notice that the allowed ranges for NP coefficients are much larger in the data-driven scenario since the uncertainties on charming penguins leak into the determination of NP Wilson coefficients.

Before concluding, we comment briefly on the possibility of a lepton universal NP contribution to C_9, that we denote here $C^{\rm NP}_{9,\rm U}$, affecting only absolute BRs and angular distributions of $b \to s\ell^+\ell^-$ decays, but leaving LUV ratios as in the SM. This possibility was already discussed in detail in Ref. [38], and the experimental situation has not changed since then. Therefore, we just summarize here the main findings of Ref. [38] for the reader's convenience. Performing a fit to experimental data within the SM in the data-driven scenario, one finds that several h_λ parameters are determined to be different from zero at 95% probability,

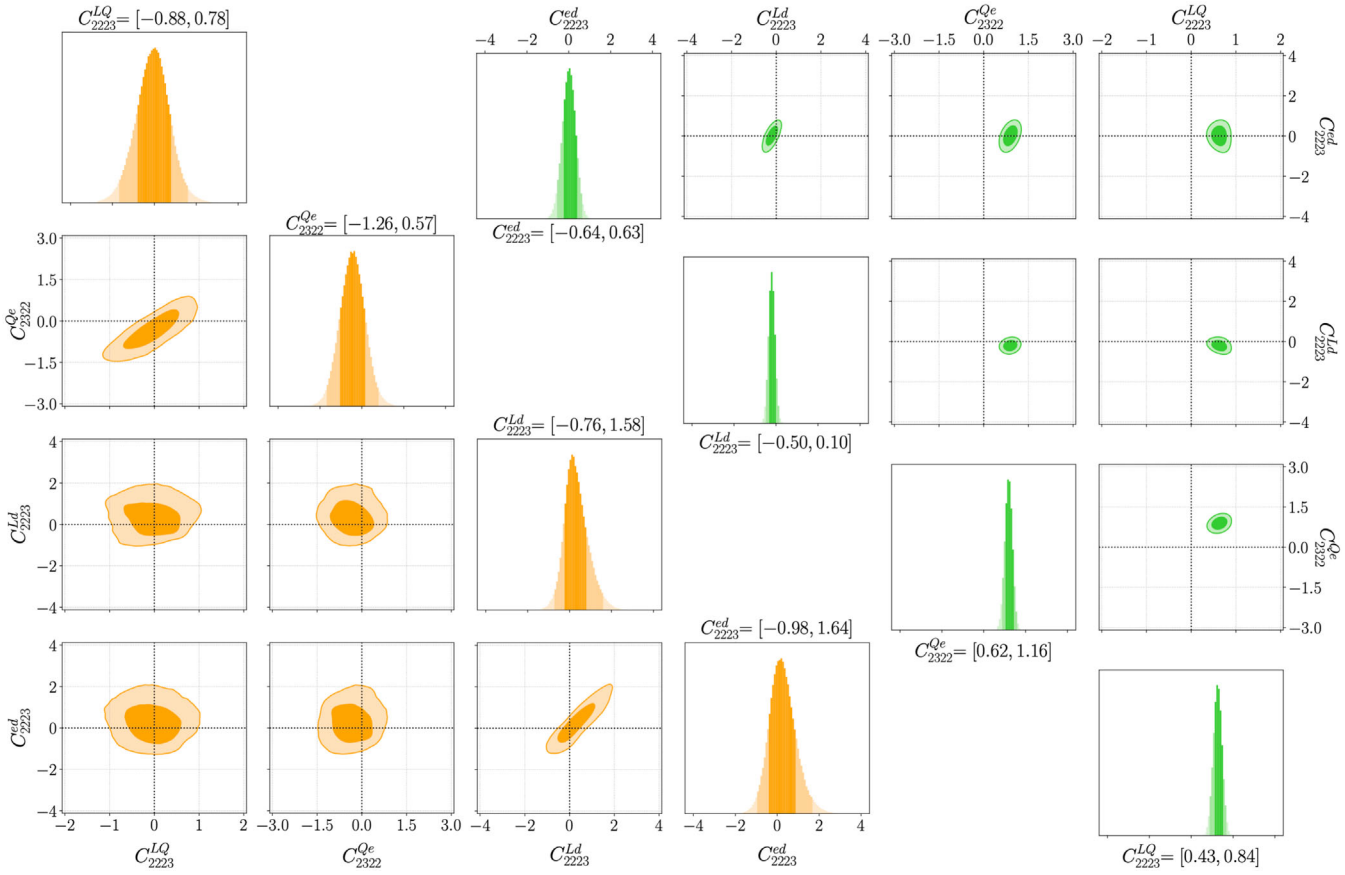

FIG. 5. Two- and one-dimensional marginalized joint PDF for the set of SMEFT Wilson coefficients C^{LQ}_{2223}, C^{Qe}_{2322}, C^{ed}_{2223}, and C^{Ld}_{2223}. For both panels, we show the 68% and 95% probability regions in green and orange on the basis of the hadronic approach adopted in the global analysis (see the text for more details).

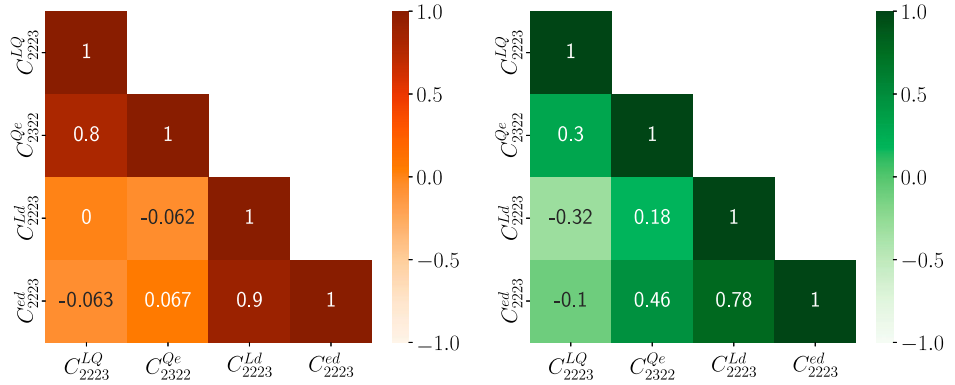

FIG. 6. Correlation matrix of the Wilson coefficients of the SMEFT operators studied in this work under the data-driven (left panel, orange) and the model-dependent (right panel, green) approaches to hadronic uncertainties in our global analysis.

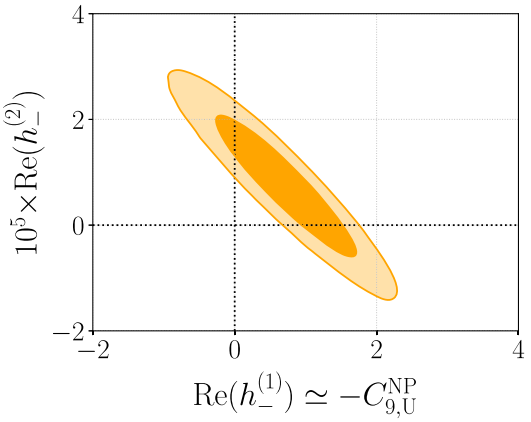

FIG. 7. Joint posterior PDF for $\mathrm{Re}(h_-^{(1)})$ and $\mathrm{Re}(h_-^{(2)})$ in a SM fit in the data-driven scenario. Darker (lighter) regions correspond to 68% (95%) probability. Notice that according to our hadronic parametrization given in Eq. (5), $\mathrm{Re}(h_-^{(1)})$ can be reinterpreted as a lepton universal NP contribution, $C_{9,\mathrm{U}}^{\mathrm{NP}}$.

supporting the picture of sizable rescattering in charming penguin amplitudes (see Table 1 in Ref. [38]). In particular, there is an interesting correlation between $\mathrm{Re}(h_-^{(1)}) \simeq -C_{9,\mathrm{U}}^{\mathrm{NP}}$ and $\mathrm{Re}(h_-^{(2)})$, as is evident from Fig. 7.[5] Data definitely require a nonvanishing combination of the two parameters; if charming penguins are treated *à la* [43–48], $\mathrm{Re}(h_-^{(2)})$ is put to zero and $\mathrm{Re}(h_-^{(1)})$ is identified with a lepton universal contribution $C_{9,\mathrm{U}}^{\mathrm{NP}}$, leading to an evidence of NP inextricably linked to the assumptions on charming-penguin amplitudes.

[5]To identify $\mathrm{Re}(h_-^{(1)})$ as $C_{9,\mathrm{U}}^{\mathrm{NP}}$, we work in the flavor $SU(3)_F$ symmetric limit, in which the same hadronic contribution affects both $B \to K^*$ and $B_s \to \phi$ transitions (see the Appendix for further details); moreover, for the sake of simplicity, we focus only on these two channels and do not take in consideration additional correlations with other hadronic parameters that similarly mimic the effect of $C_{9,\mathrm{U}}^{\mathrm{NP}}$ in $B \to K$ transitions.

Summarizing, we performed a Bayesian analysis of possible LUV NP contributions to $b \to s\ell^+\ell^-$ transitions in view of the very recent updates on $\mathrm{BR}(B_{(d,s)} \to \mu^+\mu^-)$ by the CMS Collaboration [49] and on R_K and R_{K^*} by the LHCb collaboration [54,55]. As pointed out in Refs. [24,26,30,38,40–42,91,92], the NP sensitivity of these transitions is spoilt by possible long-distance effects, see Fig. 1. Thus, in the data-driven scenario we determined simultaneously hadronic contributions, parametrized according to Eq. (4), and NP Wilson coefficients, finding no evidence for LUV NP. Conversely, evidence for NP contributions is found if charming penguins are assumed to be well described by the approach of Refs. [43–48], as reported in Tables I and II.

Finally, we considered the case of a lepton universal NP contribution to C_9, which is phenomenologically equivalent to the effect of $h_-^{(1)}$ in our data-driven analysis, confirming our previous findings in Ref. [38]; in the context of the data-driven approach, we found several hints of nonvanishing h_λ^i parameters, but no evidence of a nonvanishing $\mathrm{Re}(h_-^{(1)}) \simeq -C_{9,\mathrm{U}}^{\mathrm{NP}}$; evidence for $C_{9,\mathrm{U}}^{\mathrm{NP}}$ only arises in the model-dependent scenario in which all genuine hadronic contributions are phenomenologically negligible. Future improvements in theoretical calculations and in experimental data will hopefully allow clarifying this last point.

The work of M. F. is supported by the Deutsche Forschungsgemeinschaft (DFG, German Research Foundation) under Grant No. 396021762-TRR 257, "Particle Physics Phenomenology after the Higgs Discovery". The work of M. V. is supported by the Simons Foundation under the Simons Bridge for Postdoctoral Fellowships at SCGP and YITP, Award No. 815892. The work of A. P. is funded by Volkswagen Foundation within the initiative "Corona Crisis and Beyond—Perspectives for Science, Scholarship and Society", Grant No. 99091. A. P. was funded by the Roux Institute and the Harold Alfond Foundation. This work was supported by the Italian Ministry

of Research (MIUR) under Grant No. PRIN 20172LNEEZ. This research was supported in part through the Maxwell computational resources operated at DESY, Hamburg, Germany. M. V. wishes to thank KIT for hospitality during completion of this work.

APPENDIX

In this appendix we give further details regarding the parametrizations employed for the hadronic contributions in the data-driven and model-dependent approaches in each of the two main decays investigated in this work, namely $B \to K^* \ell\ell$ and $B \to K\ell\ell$, and how these approaches are related to each other. Concerning the third process discussed in this work, namely $B_s \to \phi\ell\ell$, we work under the assumption of $SU(3)_F$ symmetry, i.e., we consider the same hadronic contributions to $B \to K^*\ell\ell$ and $B_s \to \phi\ell\ell$. This choice is justified by the fact that it is not possible with current data to single out any $SU(3)_F$-breaking effect from $B_s \to \phi\ell\ell$, see our previous work in Ref. [38] for a detailed analysis on this matter. Starting from the model-dependent approach in the $B \to K^*$ mode, we follow the definition of Ref. [43] and give the hadronic contributions as helicity-dependent shifts in $C_{9,i}$:

$$\Delta C_{9,i}(q^2) = \frac{r_{1,i}(1-\frac{\bar{q}^2}{q^2}) + \Delta C_{9,i}(\bar{q}^2)\frac{\bar{q}^2}{q^2}}{1 + r_{2,i}\frac{\bar{q}^2-q^2}{m_{J/\psi}^2}}. \tag{A1}$$

In our fits, all the involved parameters are considered real according to the way they have been defined and computed in Ref. [43], namely by performing a Wick rotation to the Euclidean space in order to compute the light cone sum rule. In particular, they are considered flatly distributed according to the ranges given in Table 2 of the same reference, for $\bar{q}^2 = 1$. As discussed in Ref. [30], the relation between this parametrization and the one employed for the data-driven approach is given by

$$\begin{aligned}
\Delta C_{9,1}(q^2) &= -\frac{16 m_B^3 (m_B + m_{K^*})\pi^2}{\sqrt{\lambda(q^2)} V(q^2) q^2}(h_-(q^2) - h_+(q^2)) \\
\Delta C_{9,2}(q^2) &= -\frac{16 m_B^3 \pi^2}{(m_B + m_{K^*}) A_1(q^2) q^2}(h_-(q^2) + h_+(q^2)) \\
\Delta C_{9,3}(q^2) &= \frac{64\pi^2 m_B^3 m_{K^*}\sqrt{q^2}(m_B + m_{K^*})}{\lambda(q^2) A_2(q^2) q^2} h_0(q^2) \\
&\quad - \frac{16 m_B^3 (m_B + m_{K^*})(m_B^2 - q^2 - m_{K^*}^2)\pi^2}{\lambda(q^2) A_2(q^2) q^2} \\
&\quad \times (h_-(q^2) + h_+(q^2)),
\end{aligned} \tag{A2}$$

where we have introduced the helicity functions $h_\lambda(q^2)$. These functions have been defined in such a way that, in the helicity amplitudes shown in Eq. (5), the coefficients $h_{\pm}^{(0)}$ and $h_{\pm}^{(1)}$ have the same effect of a NP lepton universal shift in the real part of C_7 and C_9, namely

$$\begin{aligned}
h_-(q^2) &= -\frac{m_b}{8\pi^2 m_B}\tilde{T}_{L-}(q^2) h_{\pm}^{(0)} - \frac{\tilde{V}_{L-}(q^2)}{16\pi^2 m_B^2} h_{\pm}^{(1)} q^2 \\
&\quad + h_{\pm}^{(2)} q^4 + \mathcal{O}(q^6), \\
h_+(q^2) &= -\frac{m_b}{8\pi^2 m_B}\tilde{T}_{L+}(q^2) h_{\pm}^{(0)} - \frac{\tilde{V}_{L+}(q^2)}{16\pi^2 m_B^2} h_{\pm}^{(1)} q^2 \\
&\quad + h_+^{(0)} + h_+^{(1)} q^2 + h_+^{(2)} q^4 + \mathcal{O}(q^6), \\
h_0(q^2) &= -\frac{m_b}{8\pi^2 m_B}\tilde{T}_{L0}(q^2) h_{\pm}^{(0)} - \frac{\tilde{V}_{L0}(q^2)}{16\pi^2 m_B^2} h_{\pm}^{(1)} q^2 \\
&\quad + h_0^{(0)}\sqrt{q^2} + h_0^{(1)}(q^2)^{\frac{3}{2}} + \mathcal{O}((q^2)^{\frac{5}{2}}).
\end{aligned} \tag{A3}$$

Notice that, compared to $h_\pm$, h_0 enters the decay amplitude with an additional factor of $\sqrt{q^2}$, which is the reason why we keep only two terms in its expansion. In our fits, the parameters $h_\lambda^{(i)}$ are allowed to be complex, and we consider the following prior ranges for both their real and imaginary parts:

$$\begin{aligned}
&h_{\pm}^{(0)} \in [0, 0.1], \quad h_{\pm}^{(1)} \in [0, 4], \quad h_{\pm}^{(2)} \in [0, 10^{-4}], \\
&h_+^{(0)} \in [0, 0.0003], \quad h_+^{(1)} \in [0, 0.0005], \quad h_+^{(2)} \in [0, 10^{-4}], \\
&h_0^{(0)} \in [0, 0.002], \quad h_0^{(1)} \in [0, 0.0004].
\end{aligned} \tag{A4}$$

Such ranges have been chosen with the only requirement that increasing them would not alter the results of our fits, and are representative of our current ignorance within the data-driven approach, where we refrain ourselves from introducing any kind of theory bias other than the choice of the parametrization.

The direct comparison of the fitted results for the hadronic parameters in the two different scenarios is, for several reasons, a nontrivial task. Indeed, as explained above, the hadronic contributions are differently parametrized in the two approaches, with no trivial way to directly relate a set of parameters to the other, due in particular to the presence of form factors in Eqs. (A3) and (A4). Moreover, strong correlations as the one shown in Fig. 7 would have to be taken into account, in order to perform a fair comparison among the two scenarios. Finally, it is also important to remember that while in the model-dependent approach the hadronic parameters are taken real, this is not the case for the data-driven case where they are allowed to be complex. Nevertheless, it is still possible to circumvent all these issues in order to perform a meaningful comparison among the two approaches, by simply confronting the obtained values for $|\Delta C_{9,i}|$, in a similar fashion to what we did graphically in Fig. 3 of Ref. [38]. To this end, we report here the values obtained from the fitted value of the hadronic parameters

TABLE III. 68% HPDI for the hadronic contribution $|\Delta C_{9,1}(q^2)|$ entering in $B \to K^*$ and $B \to \phi$ transitions at different values of q^2, both in the data-driven and the model-dependent approaches. In the last column, we also report the expected size of the contributions coming from QCDF.

$\lvert\Delta C_{9,1}(q^2)\rvert$	Data driven	Model dependent	QCDF
$\lvert\Delta C_{9,1}(1.0)\rvert$	[1.58, 5.43]	[0.88, 1.08]	[0.45, 0.55]
$\lvert\Delta C_{9,1}(1.5)\rvert$	[1.23, 4.08]	[0.59, 0.73]	[0.38, 0.50]
$\lvert\Delta C_{9,1}(2.0)\rvert$	[1.00, 3.32]	[0.45, 0.56]	[0.35, 0.45]
$\lvert\Delta C_{9,1}(2.5)\rvert$	[0.82, 2.75]	[0.37, 0.46]	[0.32, 0.43]
$\lvert\Delta C_{9,1}(3.0)\rvert$	[0.66, 2.28]	[0.31, 0.40]	[0.32, 0.42]
$\lvert\Delta C_{9,1}(3.5)\rvert$	[0.53, 1.88]	[0.28, 0.36]	[0.31, 0.40]
$\lvert\Delta C_{9,1}(4.0)\rvert$	[0.44, 1.58]	[0.26, 0.34]	[0.31, 0.42]
$\lvert\Delta C_{9,1}(4.5)\rvert$	[0.41, 1.41]	[0.25, 0.33]	[0.31, 0.43]
$\lvert\Delta C_{9,1}(5.0)\rvert$	[0.45, 1.39]	[0.25, 0.33]	[0.32, 0.43]
$\lvert\Delta C_{9,1}(5.5)\rvert$	[0.57, 1.52]	[0.25, 0.33]	[0.32, 0.45]
$\lvert\Delta C_{9,1}(6.0)\rvert$	[0.75, 1.75]	[0.26, 0.35]	[0.33, 0.46]
$\lvert\Delta C_{9,1}(6.5)\rvert$	[0.95, 2.03]	[0.26, 0.35]	[0.33, 0.48]
$\lvert\Delta C_{9,1}(7.0)\rvert$	[1.15, 2.36]	[0.34, 0.43]	[0.36, 0.50]
$\lvert\Delta C_{9,1}(7.5)\rvert$	[1.36, 2.70]	[0.55, 0.66]	[0.40, 0.55]
$\lvert\Delta C_{9,1}(8.0)\rvert$	[1.55, 3.06]	[0.86, 1.01]	[0.47, 0.60]

TABLE V. 68% HPDI for the hadronic contribution $|\Delta C_{9,3}(q^2)|$ entering in $B \to K^*$ and $B \to \phi$ transitions at different values of q^2, both in the data-driven and the model-dependent approaches. In the last column, we also report the expected size of the contributions coming from QCDF.

$\lvert\Delta C_{9,3}(q^2)\rvert$	Data driven	Model dependent	QCDF
$\lvert\Delta C_{9,3}(1.0)\rvert$	[2.36, 5.98]	[0.83, 1.87]	[0.37, 0.50]
$\lvert\Delta C_{9,3}(1.5)\rvert$	[2.88, 5.75]	[0.52, 1.26]	[0.28, 0.42]
$\lvert\Delta C_{9,3}(2.0)\rvert$	[3.08, 5.54]	[0.37, 0.95]	[0.22, 0.35]
$\lvert\Delta C_{9,3}(2.5)\rvert$	[3.09, 5.28]	[0.28, 0.77]	[0.17, 0.31]
$\lvert\Delta C_{9,3}(3.0)\rvert$	[3.02, 4.98]	[0.22, 0.65]	[0.15, 0.28]
$\lvert\Delta C_{9,3}(3.5)\rvert$	[2.90, 4.66]	[0.18, 0.57]	[0.12, 0.26]
$\lvert\Delta C_{9,3}(4.0)\rvert$	[2.75, 4.33]	[0.16, 0.51]	[0.11, 0.26]
$\lvert\Delta C_{9,3}(4.5)\rvert$	[2.57, 4.02]	[0.14, 0.47]	[0.10, 0.26]
$\lvert\Delta C_{9,3}(5.0)\rvert$	[2.36, 3.73]	[0.13, 0.45]	[0.12, 0.26]
$\lvert\Delta C_{9,3}(5.5)\rvert$	[2.12, 3.48]	[0.12, 0.43]	[0.15, 0.26]
$\lvert\Delta C_{9,3}(6.0)\rvert$	[1.85, 3.27]	[0.12, 0.42]	[0.18, 0.29]
$\lvert\Delta C_{9,3}(6.5)\rvert$	[1.58, 3.11]	[0.11, 0.40]	[0.21, 0.32]
$\lvert\Delta C_{9,3}(7.0)\rvert$	[1.33, 2.99]	[0.18, 0.45]	[0.25, 0.35]
$\lvert\Delta C_{9,3}(7.5)\rvert$	[1.14, 2.92]	[0.26, 0.62]	[0.27, 0.37]
$\lvert\Delta C_{9,3}(8.0)\rvert$	[1.02, 2.90]	[0.34, 0.84]	[0.31, 0.40]

for the three $|\Delta C_{9,i}|$ in Tables III–V, for values of q^2 ranging from 1 GeV^2 to 8 GeV^2, both in the data-driven approach and in the model-dependent one. As a reference, we show also the expected size of the contributions coming from QCDF.

Concerning the $B \to K$ mode, for the model-dependent approach we include only the nonfactorizable effects coming from hard-gluon exchanges, being the soft-gluon induced terms subleading as found in Ref. [44], and $\mathcal{O}(10\%)$ of the (already small) ones introduced for the $B \to K^*$ mode and described by Eq. (A1). On the other hand, in the data-driven approach we apply the same rationale used behind Eq. (A3) and define

$$h_{B\to K}(q^2) = \frac{q^2}{m_B^2} V_L(q^2) h^{(1)}_{B\to K} + h^{(2)}_{B\to K} q^4 + \mathcal{O}(q^6). \quad \text{(A5)}$$

TABLE IV. 68% HPDI for the hadronic contribution $|\Delta C_{9,2}(q^2)|$ entering in $B \to K^*$ and $B \to \phi$ transitions at different values of q^2, both in the data-driven and the model-dependent approaches. In the last column, we also report the expected size of the contributions coming from QCDF.

$\lvert\Delta C_{9,2}(q^2)\rvert$	Data driven	Model dependent	QCDF
$\lvert\Delta C_{9,2}(1.0)\rvert$	[2.13, 4.37]	[0.54, 1.20]	[0.38, 0.46]
$\lvert\Delta C_{9,2}(1.5)\rvert$	[2.43, 4.21]	[0.35, 0.81]	[0.33, 0.41]
$\lvert\Delta C_{9,2}(2.0)\rvert$	[2.51, 4.04]	[0.25, 0.62]	[0.28, 0.37]
$\lvert\Delta C_{9,2}(2.5)\rvert$	[2.50, 3.84]	[0.19, 0.51]	[0.26, 0.33]
$\lvert\Delta C_{9,2}(3.0)\rvert$	[2.44, 3.64]	[0.16, 0.44]	[0.25, 0.33]
$\lvert\Delta C_{9,2}(3.5)\rvert$	[2.35, 3.43]	[0.13, 0.39]	[0.25, 0.33]
$\lvert\Delta C_{9,2}(4.0)\rvert$	[2.25, 3.22]	[0.12, 0.36]	[0.25, 0.33]
$\lvert\Delta C_{9,2}(4.5)\rvert$	[2.14, 3.04]	[0.11, 0.34]	[0.25, 0.34]
$\lvert\Delta C_{9,2}(5.0)\rvert$	[2.01, 2.88]	[0.11, 0.33]	[0.25, 0.35]
$\lvert\Delta C_{9,2}(5.5)\rvert$	[1.87, 2.74]	[0.11, 0.34]	[0.26, 0.36]
$\lvert\Delta C_{9,2}(6.0)\rvert$	[1.72, 2.64]	[0.11, 0.34]	[0.26, 0.36]
$\lvert\Delta C_{9,2}(6.5)\rvert$	[1.58, 2.55]	[0.11, 0.34]	[0.26, 0.37]
$\lvert\Delta C_{9,2}(7.0)\rvert$	[1.43, 2.50]	[0.20, 0.41]	[0.27, 0.38]
$\lvert\Delta C_{9,2}(7.5)\rvert$	[1.30, 2.46]	[0.34, 0.63]	[0.30, 0.42]
$\lvert\Delta C_{9,2}(8.0)\rvert$	[1.19, 2.44]	[0.55, 0.95]	[0.36, 0.46]

TABLE VI. 68% HPDI for the hadronic contribution $|\Delta C_9(q^2)|$ entering in $B \to K$ transitions at different values of q^2 in the data-driven approach. In the last column, we also report the expected size of the contributions coming from QCDF.

$\lvert\Delta C_9(q^2)\rvert$	Data driven	QCDF
$\lvert\Delta C_9(1.0)\rvert$	[2.33, 6.06]	[0.09, 0.19]
$\lvert\Delta C_9(1.5)\rvert$	[2.36, 5.97]	[0.10, 0.20]
$\lvert\Delta C_9(2.0)\rvert$	[2.41, 5.88]	[0.10, 0.20]
$\lvert\Delta C_9(2.5)\rvert$	[2.46, 5.79]	[0.11, 0.21]
$\lvert\Delta C_9(3.0)\rvert$	[2.52, 5.70]	[0.12, 0.22]
$\lvert\Delta C_9(3.5)\rvert$	[2.58, 5.63]	[0.12, 0.22]
$\lvert\Delta C_9(4.0)\rvert$	[2.65, 5.57]	[0.13, 0.23]
$\lvert\Delta C_9(4.5)\rvert$	[2.71, 5.54]	[0.13, 0.23]
$\lvert\Delta C_9(5.0)\rvert$	[2.76, 5.54]	[0.14, 0.24]
$\lvert\Delta C_9(5.5)\rvert$	[2.80, 5.57]	[0.14, 0.24]
$\lvert\Delta C_9(6.0)\rvert$	[2.83, 5.65]	[0.15, 0.25]
$\lvert\Delta C_9(6.5)\rvert$	[2.84, 5.76]	[0.16, 0.26]
$\lvert\Delta C_9(7.0)\rvert$	[2.83, 5.91]	[0.16, 0.26]
$\lvert\Delta C_9(7.5)\rvert$	[2.82, 6.10]	[0.17, 0.27]
$\lvert\Delta C_9(8.0)\rvert$	[2.80, 6.33]	[0.18, 0.28]

Once again, the parameters $h^{(i)}_{B\to K}$ are allowed to be complex, and in our fits we allow the following prior ranges for both their real and imaginary parts:

$$h^{(1)}_{B\to K} \in [0, 10], \qquad h^{(2)}_{B\to K} \in [0, 0.0002]. \tag{A6}$$

Also in this case the ranges have been chosen only taking care that they are large enough in order not to affect the results of our fits. The particularly large range for $h^{(1)}_{B\to K}$ is due to its strong correlation to $C_9^{\rm NP}$, see Fig. 5 of Ref. [38]. Similarly to what done for the $B \to K^*$ transition, we report in Table VI the fitted values for $|\Delta C_9(q^2)|$. Since, as we stated above, in the model-dependent approach we do not include the soft-gluon effects, negligible in this scenario, we report in the table only the fitted values for this hadronic correction in the data-driven approach, together with the expected size of the contributions coming from QCDF.

[1] G. Aad *et al.* (ATLAS Collaboration), Observation of a new particle in the search for the Standard Model Higgs boson with the ATLAS detector at the LHC, Phys. Lett. B **716**, 1 (2012).

[2] S. Chatrchyan *et al.* (CMS Collaboration), Observation of a new boson at a mass of 125 GeV with the CMS experiment at the LHC, Phys. Lett. B **716**, 30 (2012).

[3] R. Aaij *et al.* (LHCb Collaboration), Test of Lepton Universality Using $B^+ \to K^+\ell^+\ell^-$ Decays, Phys. Rev. Lett. **113**, 151601 (2014).

[4] R. Aaij *et al.* (LHCb Collaboration), Test of lepton universality with $B^0 \to K^{*0}\ell^+\ell^-$ decays, J. High Energy Phys. 08 (2017) 055.

[5] R. Aaij *et al.* (LHCb Collaboration), Search for Lepton-Universality Violation in $B^+ \to K^+\ell^+\ell^-$ Decays, Phys. Rev. Lett. **122**, 191801 (2019).

[6] R. Aaij *et al.* (LHCb Collaboration), Test of lepton universality in beauty-quark decays, Nat. Phys. **18**, 277 (2022).

[7] R. Aaij *et al.* (LHCb Collaboration), Tests of Lepton Universality Using $B^0 \to K^0_S\ell^+\ell^-$ and $B^+ \to K^{*+}\ell^+\ell^-$ Decays, Phys. Rev. Lett. **128**, 191802 (2022).

[8] S. Descotes-Genon, J. Matias, and J. Virto, Understanding the $B \to K^*\mu^+\mu^-$ anomaly, Phys. Rev. D **88**, 074002 (2013).

[9] W. Altmannshofer and D. M. Straub, New physics in $B \to K^*\mu\mu$?, Eur. Phys. J. C **73**, 2646 (2013).

[10] F. Beaujean, C. Bobeth, and D. van Dyk, Comprehensive Bayesian analysis of rare (semi)leptonic and radiative B decays, Eur. Phys. J. C **74**, 2897 (2014).

[11] T. Hurth and F. Mahmoudi, On the LHCb anomaly in $B \to K^*\ell^+\ell^-$, J. High Energy Phys. 04 (2014) 097.

[12] R. Aaij *et al.* (LHCb Collaboration), Differential branching fraction and angular analysis of the decay $B^0 \to K^{*0}\mu^+\mu^-$, J. High Energy Phys. 08 (2013) 131.

[13] R. Aaij *et al.* (LHCb Collaboration), Differential branching fraction and angular analysis of the decay $B^0_s \to \phi\mu^+\mu^-$, J. High Energy Phys. 07 (**2013**) 084.

[14] R. Aaij *et al.* (LHCb Collaboration), Measurement of Form-Factor-Independent Observables in the Decay $B^0 \to K^{*0}\mu^+\mu^-$, Phys. Rev. Lett. **111**, 191801 (2013).

[15] S. Chatrchyan *et al.* (CMS Collaboration), Angular analysis and branching fraction measurement of the decay $B^0 \to K^{*0}\mu^+\mu^-$, Phys. Lett. B **727**, 77 (2013).

[16] R. Aaij *et al.* (LHCb Collaboration), Differential branching fractions and isospin asymmetries of $B \to K^{(*)}\mu^+\mu^-$ decays, J. High Energy Phys. 06 (2014) 133.

[17] R. Aaij *et al.* (LHCb Collaboration), Angular analysis and differential branching fraction of the decay $B^0_s \to \phi\mu^+\mu^-$, J. High Energy Phys. 09 (2015) 179.

[18] R. Aaij *et al.* (LHCb Collaboration), Angular analysis of the $B^0 \to K^{*0}\mu^+\mu^-$ decay using 3 fb^{-1} of integrated luminosity, J. High Energy Phys. 02 (2016) 104.

[19] R. Aaij *et al.* (LHCb Collaboration), Measurement of CP-Averaged Observables in the $B^0 \to K^{*0}\mu^+\mu^-$ Decay, Phys. Rev. Lett. **125**, 011802 (2020).

[20] A. M. Sirunyan *et al.* (CMS Collaboration), Angular analysis of the decay $B^+ \to K^*(892)^+\mu^+\mu^-$ in proton-proton collisions at $\sqrt{s} = 8$ TeV, J. High Energy Phys. 04 (2021) 124.

[21] R. Aaij *et al.* (LHCb Collaboration), Angular Analysis of the $B^+ \to K^{*+}\mu^+\mu^-$ Decay, Phys. Rev. Lett. **126**, 161802 (2021).

[22] R. Aaij *et al.* (LHCb Collaboration), Branching Fraction Measurements of the Rare $B^0_s \to \phi\mu^+\mu^-$ and $B^0_s \to f'_2(1525)\mu^+\mu^-$ Decays, Phys. Rev. Lett. **127**, 151801 (2021).

[23] R. Aaij *et al.* (LHCb Collaboration), Angular analysis of the rare decay $B^0_s \to \phi\mu^+\mu^-$, J. High Energy Phys. 11 (2021) 043.

[24] S. Jäger and J. Martin Camalich, On $B \to V\ell\ell$ at small dilepton invariant mass, power corrections, and new physics, J. High Energy Phys. 05 (2013) 043.

[25] S. Descotes-Genon, L. Hofer, J. Matias, and J. Virto, On the impact of power corrections in the prediction of $B \to K^*\mu^+\mu^-$ observables, J. High Energy Phys. 12 (2014) 125.

[26] S. Jäger and J. Martin Camalich, Reassessing the discovery potential of the $B \to K^*\ell^+\ell^-$ decays in the large-recoil region: SM challenges and BSM opportunities, Phys. Rev. D **93**, 014028 (2016).

[27] M. Ciuchini, E. Franco, G. Martinelli, and L. Silvestrini, Charming penguins in B decays, Nucl. Phys. **B501**, 271 (1997).

[28] J. Lyon and R. Zwicky, Resonances gone topsy turvy—The charm of QCD or new physics in $b \to s\ell^+\ell^-$?, arXiv:1406.0566.

[29] D. Melikhov, Nonfactorizable charming loops in FCNC B decays versus B-decay semileptonic form factors, Phys. Rev. D **106**, 054022 (2022).

[30] M. Ciuchini, M. Fedele, E. Franco, S. Mishima, A. Paul, L. Silvestrini, and M. Valli, $B \to K^* \ell^+ \ell^-$ decays at large recoil in the Standard Model: A theoretical reappraisal, J. High Energy Phys. 06 (**2016**) 116.

[31] G. Hiller, D. Loose, and I. Nišandžić, Flavorful leptoquarks at the LHC and beyond: Spin 1, J. High Energy Phys. 06 (2021) 080.

[32] L.-S. Geng, B. Grinstein, S. Jäger, S.-Y. Li, J. Martin Camalich, and R.-X. Shi, Implications of new evidence for lepton-universality violation in $B^+ \to K^+ \ell^+ \ell^-$-decays, Phys. Rev. D **104**, 035029 (2021).

[33] C. Cornella, D. A. Faroughy, J. Fuentes-Martin, G. Isidori, and M. Neubert, Reading the footprints of the B-meson flavor anomalies, J. High Energy Phys. 08 (2021) 050.

[34] T. Hurth, F. Mahmoudi, D. M. Santos, and S. Neshatpour, More indications for lepton nonuniversality in $b \to s \ell^+ \ell^-$, Phys. Lett. B **824**, 136838 (2022).

[35] M. Algueró, B. Capdevila, S. Descotes-Genon, J. Matias, and M. Novoa-Brunet, $b \to s \ell^+ \ell^-$ global fits after R_{K_S} and $R_{K^{*+}}$, Eur. Phys. J. C **82**, 326 (2022).

[36] R. Bause, H. Gisbert, M. Golz, and G. Hiller, Interplay of dineutrino modes with semileptonic rare B-decays, J. High Energy Phys. 12 (2021) 061.

[37] W. Altmannshofer and P. Stangl, New physics in rare B decays after Moriond 2021, Eur. Phys. J. C **81**, 952 (2021).

[38] M. Ciuchini, M. Fedele, E. Franco, A. Paul, L. Silvestrini, and M. Valli, Charming penguins and lepton universality violation in $b \to s \ell^+ \ell^-$ decays, Eur. Phys. J. C **83**, 64 (2023).

[39] M. Algueró, J. Matias, B. Capdevila, and A. Crivellin, Disentangling lepton flavor universal and lepton flavor universality violating effects in $b \to s \ell^+ \ell^-$ transitions, Phys. Rev. D **105**, 113007 (2022).

[40] M. Ciuchini, A. M. Coutinho, M. Fedele, E. Franco, A. Paul, L. Silvestrini, and M. Valli, On flavourful Easter eggs for New Physics hunger and lepton flavour universality violation, Eur. Phys. J. C **77**, 688 (2017).

[41] M. Ciuchini, A. M. Coutinho, M. Fedele, E. Franco, A. Paul, L. Silvestrini, and M. Valli, New Physics in $b \to s \ell^+ \ell^-$ confronts new data on lepton universality, Eur. Phys. J. C **79**, 719 (2019).

[42] M. Ciuchini, M. Fedele, E. Franco, A. Paul, L. Silvestrini, and M. Valli, Lessons from the $B^{0,+} \to K^{*0,+} \mu^+ \mu^-$ angular analyses, Phys. Rev. D **103**, 015030 (2021).

[43] A. Khodjamirian, T. Mannel, A. Pivovarov, and Y.-M. Wang, Charm-loop effect in $B \to K^{(*)} \ell^+ \ell^-$ and $B \to K^* \gamma$, J. High Energy Phys. 09 (2010) 089.

[44] A. Khodjamirian, T. Mannel, and Y. M. Wang, $B \to K \ell^+ \ell^-$ decay at large hadronic recoil, J. High Energy Phys. 02 (2013) 010.

[45] C. Bobeth, M. Chrzaszcz, D. van Dyk, and J. Virto, Long-distance effects in $B \to K^* \ell \ell$ from analyticity, Eur. Phys. J. C **78**, 451 (2018).

[46] M. Chrzaszcz, A. Mauri, N. Serra, R. Silva Coutinho, and D. van Dyk, Prospects for disentangling long- and short-distance effects in the decays $B \to K^* \mu^+ \mu^-$, J. High Energy Phys. 10 (2019) 236.

[47] N. Gubernari, D. van Dyk, and J. Virto, Non-local matrix elements in $B_{(s)} \to \{K^{(*)}, \phi\} \ell^+ \ell^-$, J. High Energy Phys. 02 (2021) 088.

[48] N. Gubernari, M. Reboud, D. van Dyk, and J. Virto, Improved theory predictions and global analysis of exclusive $b \to s \mu^+ \mu^-$ processes, J. High Energy Phys. 09 (2022) 133.

[49] CMS Collaboration, Measurement of $\mathrm{B}_\mathrm{s}^0 \to \mu^+ \mu^-$ decay properties and search for the $\mathrm{B}^0 \to \mu\mu$ decay in proton-proton collisions at $\sqrt{s} = 13$ TeV, Report No. CMS-PAS-BPH-21-006, 2022.

[50] C. Bobeth, M. Gorbahn, T. Hermann, M. Misiak, E. Stamou, and M. Steinhauser, $B_{s,d} \to l^+ l^-$ in the Standard Model with Reduced Theoretical Uncertainty, Phys. Rev. Lett. **112**, 101801 (2014).

[51] M. Bona *et al.* (UTfit Collaboration), New UTfit analysis of the unitarity triangle in the Cabibbo-Kobayashi-Maskawa scheme, arXiv:2212.03894.

[52] R. Alonso, B. Grinstein, and J. Martin Camalich, $SU(2) \times U(1)$ Gauge Invariance and the Shape of New Physics in Rare B Decays, Phys. Rev. Lett. **113**, 241802 (2014).

[53] R. Fleischer, R. Jaarsma, and G. Tetlalmatzi-Xolocotzi, In pursuit of new physics with $B^0_{s,d} \to \ell^+ \ell^-$, J. High Energy Phys. 05 (2017) 156.

[54] LHCb Collaboration, Test of lepton universality in $b \to s \ell^+ \ell^-$ decays, arXiv:2212.09152.

[55] LHCb Collaboration, Measurement of lepton universality parameters in $B^+ \to K^+ \ell^+ \ell^-$ and $B^0 \to K^{*0} \ell^+ \ell^-$ decays, arXiv:2212.09153.

[56] A. Crivellin and M. Hoferichter, Hints of lepton flavor universality violations, Science **374**, 1051 (2021).

[57] A. J. Buras and J. Girrbach, Left-handed Z' and Z FCNC quark couplings facing new $b \to s \mu^+ \mu^-$ data, J. High Energy Phys. 12 (2013) 009.

[58] A. J. Buras, F. De Fazio, and J. Girrbach-Noe, Z-Z' mixing and Z-mediated FCNCs in $SU(3)_C \times SU(3)_L \times U(1)_X$ models, J. High Energy Phys. 08 (2014) 039.

[59] W. Altmannshofer, S. Gori, M. Pospelov, and I. Yavin, Quark flavor transitions in $L_\mu - L_\tau$ models, Phys. Rev. D **89**, 095033 (2014).

[60] S. L. Glashow, D. Guadagnoli, and K. Lane, Lepton Flavor Violation in B Decays?, Phys. Rev. Lett. **114**, 091801 (2015).

[61] B. Gripaios, M. Nardecchia, and S. A. Renner, Composite leptoquarks and anomalies in B-meson decays, J. High Energy Phys. 05 (2015) 006.

[62] R. Barbieri, C. W. Murphy, and F. Senia, B-decay anomalies in a composite leptoquark model, Eur. Phys. J. C **77**, 8 (2017).

[63] N. Assad, B. Fornal, and B. Grinstein, Baryon number and lepton universality violation in leptoquark and diquark models, Phys. Lett. B **777**, 324 (2018).

[64] L. Di Luzio, A. Greljo, and M. Nardecchia, Gauge leptoquark as the origin of B-physics anomalies, Phys. Rev. D **96**, 115011 (2017).

[65] L. Calibbi, A. Crivellin, and T. Li, Model of vector leptoquarks in view of the B-physics anomalies, Phys. Rev. D **98**, 115002 (2018).

[66] M. Bordone, C. Cornella, J. Fuentes-Martin, and G. Isidori, A three-site gauge model for flavor hierarchies and flavor anomalies, Phys. Lett. B **779**, 317 (2018).

[67] R. Barbieri and A. Tesi, B-decay anomalies in Pati-Salam SU(4), Eur. Phys. J. C **78**, 193 (2018).

[68] A. Greljo and B. A. Stefanek, Third family quark–lepton unification at the TeV scale, Phys. Lett. B **782**, 131 (2018).

[69] D. Marzocca, Addressing the B-physics anomalies in a fundamental composite Higgs model, J. High Energy Phys. 07 (2018) 121.

[70] L. Di Luzio, J. Fuentes-Martin, A. Greljo, M. Nardecchia, and S. Renner, Maximal flavour violation: A Cabibbo mechanism for leptoquarks, J. High Energy Phys. 11 (2018) 081.

[71] M. Blanke and A. Crivellin, B Meson Anomalies in a Pati-Salam Model within the Randall-Sundrum Background, Phys. Rev. Lett. **121**, 011801 (2018).

[72] B. Fornal, S. A. Gadam, and B. Grinstein, Left-right SU(4) vector leptoquark model for flavor anomalies, Phys. Rev. D **99**, 055025 (2019).

[73] P. Arnan, A. Crivellin, M. Fedele, and F. Mescia, Generic loop effects of new scalars and fermions in $b \to s\ell^+\ell^-$, $(g-2)_\mu$ and a vector-like 4$^{\text{th}}$ generation, J. High Energy Phys. 06 (2019) 118.

[74] J. Fuentes-Martín and P. Stangl, Third-family quark-lepton unification with a fundamental composite Higgs, Phys. Lett. B **811**, 135953 (2020).

[75] V. Gherardi, D. Marzocca, and E. Venturini, Low-energy phenomenology of scalar leptoquarks at one-loop accuracy, J. High Energy Phys. 01 (2021) 138.

[76] G. Arcadi, L. Calibbi, M. Fedele, and F. Mescia, Muon $g-2$ and B-Anomalies from Dark Matter, Phys. Rev. Lett. **127**, 061802 (2021).

[77] L. Darmé, M. Fedele, K. Kowalska, and E. M. Sessolo, Flavour anomalies and the muon $g-2$ from feebly interacting particles, J. High Energy Phys. 03 (2022) 085.

[78] A. Greljo, Y. Soreq, P. Stangl, A. E. Thomsen, and J. Zupan, Muonic force behind flavor anomalies, J. High Energy Phys. 04 (2022) 151.

[79] J. Davighi and J. Tooby-Smith, Electroweak flavour unification, J. High Energy Phys. 09 (2022) 193.

[80] J. Davighi, A. Greljo, and A. E. Thomsen, Leptoquarks with exactly stable protons, Phys. Lett. B **833**, 137310 (2022).

[81] J. Fuentes-Martin, G. Isidori, J. M. Lizana, N. Selimovic, and B. A. Stefanek, Flavor hierarchies, flavor anomalies, and Higgs mass from a warped extra dimension, Phys. Lett. B **834**, 137382 (2022).

[82] W. Buchmuller and D. Wyler, Effective lagrangian analysis of new interactions and flavor conservation, Nucl. Phys. **B268**, 621 (1986).

[83] B. Grzadkowski, M. Iskrzynski, M. Misiak, and J. Rosiek, Dimension-six terms in the Standard Model Lagrangian, J. High Energy Phys. 10 (**2010**) 085.

[84] J. Gratrex, M. Hopfer, and R. Zwicky, Generalised helicity formalism, higher moments and the $B \to K_{J_K}(\to K\pi)\bar{\ell}_1\ell_2$ angular distributions, Phys. Rev. D **93**, 054008 (2016).

[85] G. Buchalla, A. J. Buras, and M. E. Lautenbacher, Weak decays beyond leading logarithms, Rev. Mod. Phys. **68**, 1125 (1996).

[86] B. Grinstein, TASI-2013 lectures on flavor physics, in *Proceedings of the Theoretical Advanced Study Institute in Elementary Particle Physics: Particle Physics: The Higgs Boson and Beyond (TASI 2013) Boulder, Colorado, 2013* (2015), arXiv:1501.05283.

[87] L. Silvestrini, Effective theories for quark flavour physics, in *Effective Field Theory in Particle Physics and Cosmology* (Oxford University Press, 2020).

[88] A. Bharucha, D. M. Straub, and R. Zwicky, $B \to V\ell^+\ell^-$ in the Standard Model from light-cone sum rules, J. High Energy Phys. 08 (2016) 098.

[89] N. Gubernari, A. Kokulu, and D. van Dyk, $B \to P$ and $B \to V$ form factors from B-meson light-cone sum rules beyond leading twist, J. High Energy Phys. 01 (2019) 150.

[90] V. G. Chobanova, T. Hurth, F. Mahmoudi, D. Martinez Santos, and S. Neshatpour, Large hadronic power corrections or new physics in the rare decay $B \to K^*\mu^+\mu^-$?, J. High Energy Phys. 07 (**2017**) 025.

[91] M. Ciuchini, M. Fedele, E. Franco, S. Mishima, A. Paul, L. Silvestrini *et al.*, $B \to K^*\ell^+\ell^-$ in the Standard Model: Elaborations and interpretations, Proc. Sci. ICHEP2016 (**2016**) 584 [arXiv:1611.04338].

[92] M. Ciuchini, A. M. Coutinho, M. Fedele, E. Franco, A. Paul, L. Silvestrini *et al.*, Hadronic uncertainties in semileptonic $B \to K^*\mu^+\mu^-$ decays, Proc. Sci. BEAUTY2018 (**2018**) 044 [arXiv:1809.03789].

[93] M. Ladisa and P. Santorelli, The role of long distance contribution to the $B \to K^{(*)}\ell^+\ell^-$ in the Standard Model, arXiv:2208.00080.

[94] M. Ablikim *et al.* (BESIII Collaboration), Observation of a Near-Threshold Structure in the K^+ Recoil-Mass Spectra in $e^+e^- \to K^+(D_s^-D^{*0} + D_s^{*-}D^0)$, Phys. Rev. Lett. **126**, 102001 (2021).

[95] C. Fronsdal and R. E. Norton, Integral representations for vertex functions, J. Math. Phys. (N.Y.) **5**, 100 (1964).

[96] A. Celis, J. Fuentes-Martin, A. Vicente, and J. Virto, Gauge-invariant implications of the LHCb measurements on lepton-flavor nonuniversality, Phys. Rev. D **96**, 035026 (2017).

[97] L. Alasfar, A. Azatov, J. de Blas, A. Paul, and M. Valli, B anomalies under the lens of electroweak precision, J. High Energy Phys. 12 (2020) 016.

[98] J. Aebischer, A. Crivellin, M. Fael, and C. Greub, Matching of gauge invariant dimension-six operators for $b \to s$ and $b \to c$ transitions, J. High Energy Phys. 05 (2016) 037.

[99] V. Khachatryan *et al.* (CMS and LHCb Collaborations), Observation of the rare $B_s^0 \to \mu^+\mu^-$ decay from the combined analysis of CMS and LHCb data, Nature (London) **522**, 68 (2015).

[100] R. Aaij *et al.* (LHCb Collaboration), Measurement of the $B_s^0 \to \mu^+\mu^-$ branching fraction and effective lifetime and search for $B^0 \to \mu^+\mu^-$ decays, Phys. Rev. Lett. **118**, 191801 (2017).

[101] M. Aaboud *et al.* (ATLAS Collaboration), Study of the rare decays of B_s^0 and B^0 mesons into muon pairs using data collected during 2015 and 2016 with the ATLAS detector, J. High Energy Phys. 04 (2019) 098.

[102] A. M. Sirunyan *et al.* (CMS Collaboration), Measurement of properties of $B_s^0 \to \mu^+\mu^-$ decays and search for $B^0 \to \mu^+\mu^-$ with the CMS experiment, J. High Energy Phys. 04 (2020) 188.

[103] R. Aaij *et al.* (LHCb Collaboration), Analysis of Neutral B-Meson Decays into Two Muons, Phys. Rev. Lett. **128**, 041801 (2022).

[104] S. Wehle *et al.* (Belle Collaboration), Lepton-Flavor-Dependent Angular Analysis of $B \to K^* \ell^+ \ell^-$, Phys. Rev. Lett. **118**, 111801 (2017).

[105] A. Abdesselam *et al.* (Belle Collaboration), Test of Lepton-Flavor Universality in $B \to K^* \ell^+ \ell^-$ Decays at Belle, Phys. Rev. Lett. **126**, 161801 (2021).

[106] J. De Blas *et al.*, HEPfit: A code for the combination of indirect and direct constraints on high energy physics models, Eur. Phys. J. C **80**, 456 (2020).

[107] HEPfit: A tool to combine indirect and direct constraints on high energy physics. http://hepfit.roma1.infn.it/.

[108] M. Beneke, T. Feldmann, and D. Seidel, Exclusive radiative and electroweak $b \to d$ and $b \to s$ penguin decays at NLO, Eur. Phys. J. C **41**, 173 (2005).

[109] T. Ando, Predictive Bayesian model selection, Am. J. Math. Manage. Sci. **31**, 13 (2011).

[110] R. E. Kass and A. E. Raftery, Bayes factors, J. Am. Stat. Assoc. **90**, 773 (1995).

[111] G. Hiller and M. Schmaltz, R_K and future $b \to s\ell\ell$ physics beyond the standard model opportunities, Phys. Rev. D **90**, 054014 (2014).